IOPscience iopscience.iop.org

Home Search Collections Journals About Contact us My IOPscience

Effects of spin frustration in $YBa_2Cu_3O_{6+x}$

This article has been downloaded from IOPscience. Please scroll down to see the full text article.

1990 J. Phys.: Condens. Matter 2 9423

(http://iopscience.iop.org/0953-8984/2/47/016)

View the table of contents for this issue, or go to the journal homepage for more

Download details:
IP Address: 171.66.16.151
The article was downloaded on 11/05/2010 at 07:00

Please note that terms and conditions apply.

J. Phys.: Condens. Matter 2 (1990) 9423–9433. Printed in the UK

Effects of spin frustration in $YBa_2Cu_3O_{6+x}$

Yong Lu and Bruce R Patton
Department of Physics, The Ohio State University, Columbus, OH 43210, USA

Received 18 April 1990

Abstract. An Ising spin model for the magnetic phase of $YBa_2Cu_3O_{6+x}$ (123) is studied with Monte Carlo simulations. The existence of frustrated spin couplings is shown to play an important role in the spin ordering. The specific heat, magnetic order parameters and susceptibility are calculated for various values of x. The deduced magnetic phase diagram is in good agreement with experimental results, showing the interplay between type-I and type-II antiferromagnetic orders. The relevance to a variety of doped 123 materials is discussed with a more general three-dimensional phase diagram.

1. Introduction

The effect of frustration in determining the nature of magnetic ordering in spin systems has been studied in a variety of models [1]. Frustrated spin systems are known to give rise to a rich variety of non-trivial possibilities, including all combinations of finite or vanishing zero-temperature entropy and finite or zero transition temperatures.

The most recent examples of frustrated spin systems under intensive investigation are magnetic phases of the high transition temperature (T_c) superconductors. They have attracted much attention because in such systems magnetic properties are believed to be directly related to the origin of the superconductivity [2]. Magnetic susceptibility and neutron scattering experiments done on these materials have shown that their magnetic properties depend strongly on the oxygen content x. $YBa_2Cu_3O_{6+x}$ for $x = 0$ is a simple antiferromagnet, while for $x > 0.5$ it is a superconductor with no evidence of magnetic long-range order (LRO). For intermediate values of x, the material shows a variety of different magnetic phases, and is not yet completely understood [3–7]

To study the possible role of various types of frustration in the three-dimensional (3D) spin ordering seen in $YBa_2Cu_3O_{6+x}$ with neutron scattering, we consider here a simple classical Ising spin model. The advantage of the Ising approach is that the effects of frustration are generally largest in this case, and therefore provide an upper bound for the effects under consideration.

In addition the Ising model may be relevant to the high-T_c materials. Although the Cu^{2+} ion in the copper-oxide materials is expected to be very isotropic in spin space, small anisotropies may still lead to easy axis or easy plane behaviour, thus making the Ising model results relevant, as in the case of K_2NiF_4 [8]. Neutron scattering has revealed some small anisotropy in spin space in both La_2CuO_4 and $YBa_2Cu_3O_{6+x}$, with ordered spins confined to a particular direction or plane [5, 9], consistent with the fact that in the presence of long-range order, even a small anisotropy reduces the spin

0953-8984/90/479423+11$03.50 © 1990 IOP Publishing Ltd

symmetry. Therefore, in high-T_C materials, although spins are believed to be more Heisenberg in character near the Néel temperature T_N[9,10], they may develop Ising (or XY) like symmetry at low temperatures.

Frustrated spin interactions in our model are introduced when extra oxygen is doped into $YBa_2Cu_3O_6$. The concentration of oxygen plays a key role in determining the valence states of the Cu ions, and therefore the location of spins in the lattice and the exchange interactions between them. To model the magnetic lattice, we attach a single Ising spin to every Cu^{2+} in the lattice, incorporate appropriate exchange couplings between spins, and then use Monte Carlo simulations to calculate quantities of interest, such as specific heat, susceptibility and order parameters [11].

In this paper, we present the results of our Monte Carlo study on the frustrated Ising model. In section 2, we construct the model with consideration of what is known about the structure of $YBa_2Cu_3O_{6+x}$. In section 3, we discuss how the Monte Carlo simulations are carried out and the physical implications of the results. Conclusions and a summary are presented in section 4. Corresponding results for the XY and Heisenberg models will be presented elsewhere [12].

2. The frustrated Ising model

The lattice on which the spins may reside consists of the Cu sites in $YBa_2Cu_3O_{6+x}$, which has a layered structure as shown in figure 1. The Ising Hamiltonian we use takes the following form

$$H = \sum_{i,j} J_{ij} S_i S_j \tag{1}$$

where the indices i and j label only the spin sites where a Cu^{2+} ion resides. The spin density on each layer, the exchange couplings J_{ij} and the degree of frustration are all determined by the oxygen content x.

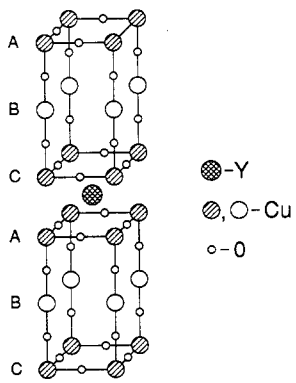

Figure 1. The lattice structure of $YBa_2Cu_3O_{6+x}$ shown on two unit cells. At $x = 0$, only (hatched) Cu sites on A and C have spins, and there is no oxygens on B.

First we discuss how the density of spins is changed by the oxygen content x. At $x = 0$, experiments show that $YBa_2Cu_3O_6$ is a magnetic insulator [13] in which the B

layers contain only non-magnetic Cu^{1+} ions, while the CuO_2 planes A and C contain only magnetic Cu^{2+} ions, due to the higher oxygen coordination [14, 15]†. Thus, at $x = 0$, there is a spin at every Cu site on the A and C layers, but none on the B. As x increases from 0, each additional O^{2-} contributes two holes to the lattice. A hole added to a Cu^{1+} ion on B creates a Cu^{2+} with a spin; while a hole entering the A or C layers is believed to sit on an O site and to eliminate a neighbour Cu^{2+} spin through the formation of a singlet spin state [16]‡. At a given oxygen doping concentration x, the total number of additional holes is $2x$ per unit cell, which we divide into f per unit cell on B and $(x - f/2)$ equally on A and C respectively. Here f is introduced as the number of holes per unit cell (out of the total $2x$) going into the B layers and satisfies $0 \leq f \leq 2x$. In the present work, we consider the quenched case with a random distribution of O^{2-} on the B layers, at a given oxygen concentration x. The quenched model is thus characterized by a random distribution, on the lattice shown in figure 1, of n_{AC} spins per unit cell in A or C ($n_{AC} = n_A = n_C$) and n_B spins per unit cell in B, with

$$\begin{aligned} n_{AC} &= 1 - (x - f/2) \\ n_B &= f. \end{aligned} \tag{2}$$

In general, unless the material is rapidly quenched, correlations will exist among the O^{2-} ions on the B layers, resulting as $x \rightarrow 1$ in ordering along a preferred chain direction and a transition to an orthorhombic structure.

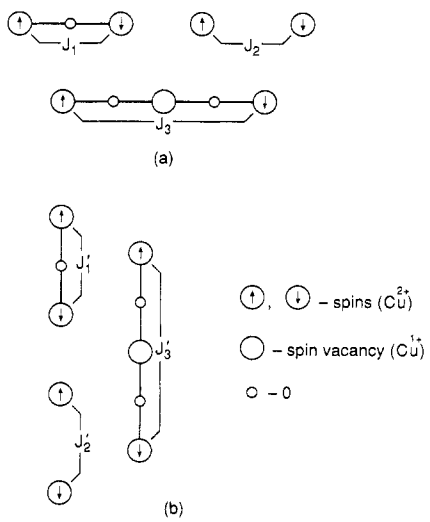

Figure 2. (a) The three different types of *intralayer* couplings and (b) the three different types of *interlayer* couplings.

Now we consider the exchange couplings J_{ij} present in the model. As shown in figure 2, all the *interlayer* couplings are noted with a superscript 'prime' and

† It may be possible to produce spins on the B layers for $x = 0$, by replacing the Y atom with Nd; see [7].

‡ The added hole on the A/C plane could also form a Cu^{3+} ion; however, there is little evidence for the trivalent Cu ion in this system or in similar environments, see [17].

all the *intralayer* couplings without. At $x = 0$, three different couplings are required by the ordered spin configuration seen in neutron scattering [5]: J_1 is the intralayer nearest-neighbour superexchange coupling through an O^{2-}; J_2' is the interlayer nearest-neighbour coupling between adjoining A and C layers; J_3' is the other long-range coupling between the A and C through the B layer. For $x > 0$, the spins on the B and spin vacancies on the A a nd C bring in three more couplings: an interlayer superexchange coupling J_1' between a spin on the B and a nearest neighbours on the A or C, which replaces J_3'; an intralayer next-nearest-neighbour coupling J_3 in the A or C through a spin vacancy site, analogous to the interlayer J_3'; an intralayer nearest-neighbour J_2 in B without an intervening O^{2-} in between†, analogous to the interlayer J_2'. All these couplings are antiferromagnetic (AF) except J_1', which is not yet clearly known to be ferromagnetic or antiferromagnetic, but either sign for J_1' would give the same effective ferromagnetic coupling between the A and C, which frustrates the AF coupling J_3'.

The effects of frustration can be easily seen by looking at the competing couplings, J_1' and J_3', and also J_1 and J_3. The competition between J_1 and J_3 weakens the two-dimensional (2D) AF order in the A or C layers, while the competition between J_1' and J_3' has an even more dramatic effect. At $x = 0$, the order along the c direction is determined by J_3', together with J_2', forming the so-called type-I order with the period of the unit cell c_0, where c_0 is the lattice constant in the c direction. Thus A and C order antiferromagnetically within a unit cell. As x increases from 0, J_1' starts to compete with J_3' in the c direction, tending to form the so-called type-II order with period $2c_0$, thus A and C order *ferromagnetically* within a unit cell. We therefore define two different 3D AF order parameters to describe the 3D AF LRO in the system. Type I order is described by

$$l_{\mathrm{I}} = \sum_n (m_{\mathrm{A}}^{\dagger} - m_{\mathrm{C}}^{\dagger}) \tag{3}$$

where $m_{\mathrm{A}}^{\dagger}$ and $m_{\mathrm{C}}^{\dagger}$ are the 2D *staggered* magnetization on the A and C layers respectively, and n labels the unit cells in the c direction. The order parameter l_{I} equals unity for the AF order observed at $x = 0$. Type-II order is described by

$$l_{\mathrm{II}} = \sum_n (-1)^n (m_{\mathrm{A}}^{\dagger} - m_{\mathrm{B}}^{\dagger} + m_{\mathrm{C}}^{\dagger}) \tag{4}$$

where $m_{\mathrm{B}}^{\dagger}$ is the 2D staggered magnetization on the B layers; and l_{II} is non-zero when type-II order is present.

The MC simulations are carried out on a 12 × 12 × 6 (unit cell) lattice, which contains 1728 spins at $x = 0$, with 2000 to 20000 MC steps per spin depending on the equilibration time of the system. To assign numerical values for the various couplings J discussed in the above, we note that, from type of the exchange, bond length and symmetry of valence electron orbital, the relative magnitude of these different couplings may be determined: for intralayer couplings, J_1 should be larger than J_2 and J_3; for interlayer couplings, J_1' should be larger than J_2' and J_3'; all intralayer couplings should be much larger than the corresponding interlayer couplings. More

† We put spins randomly on B, and approximate nearest neighbour coupling by an average of J_1 and J_2 weighted by number of bonds occupied by O^{2-}.

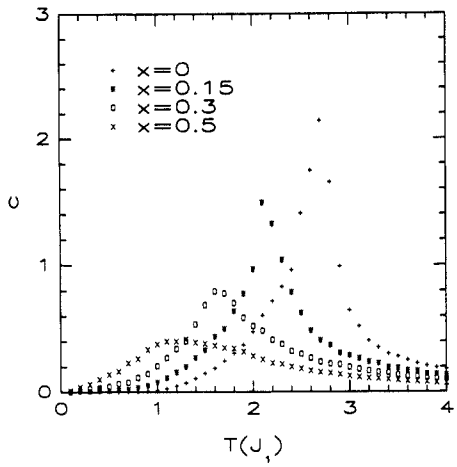

Figure 3. Specific heat (per spin) c versus temperature T for various values of oxygen doping x.

quantitative analysis can be found in [18] and [19]. Taking all these considerations into account, the interactions parameters are chosen, in units of J_1, to be

$$\begin{aligned} J_1 &= 1 & J_1' &= 0.4 \\ J_2 &= 0.2 & J_2' &= 0.2 \\ J_3 &= 0.25 & J_3' &= 0.1. \end{aligned} \tag{5}$$

In the next section, we will discuss the results of our simulation with the distribution of spins in the lattice determined by (2) and supplemented by the condition

$$f = 0.4x \tag{6}$$

which is chosen so that AF LRO disappears at $x \approx 0.5$. This spin distribution gives a phase diagram in a good agreement with the neutron scattering experiments on $YBa_2Cu_3O_{6+x}$. Equation (6) gives more holes on A and C layers than the x-ray absorption experiments suggested [20], because the classical Ising model neglects charge fluctuations and overestimates magnetic correlations. We also performed the simulations with different spin distributions corresponding to $f = 0$ and $f = 2x$, which we will discuss in the last section.

We would like to emphasize here that the qualitative picture following from our calculations does not depend sensitively on the magnitudes of J's and the spin distribution. As we will discuss in the last section, deviations from the choice listed in (5) and (6) only move phase boundaries smoothly in the parameter space.

3. Results and discussion

The results from the simulations include the following: the specific heat, the magnetic susceptibility and the order parameters l_{I} and l_{II} as functions of temperature at different oxygen content x. In figures 3 and 4, the specific heat and the AF order parameters l_{I} and l_{II} are shown as functions of temperature T for various x, while figure 5 shows the magnetic susceptibility.

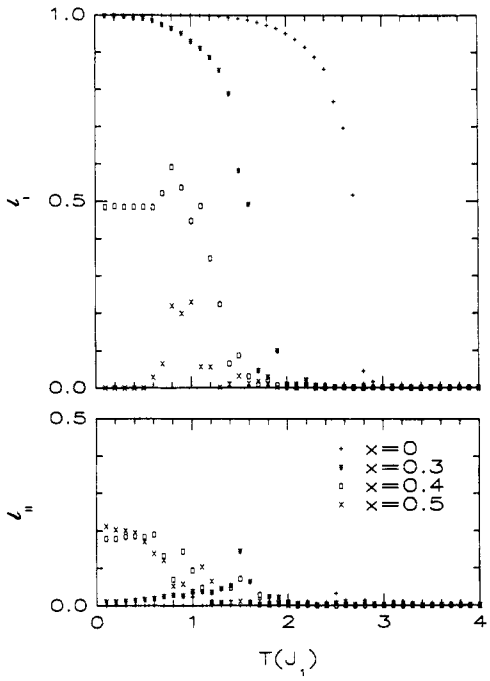

Figure 4. The AF order parameters l_{I} and l_{II} versus temperature T for various values of x.

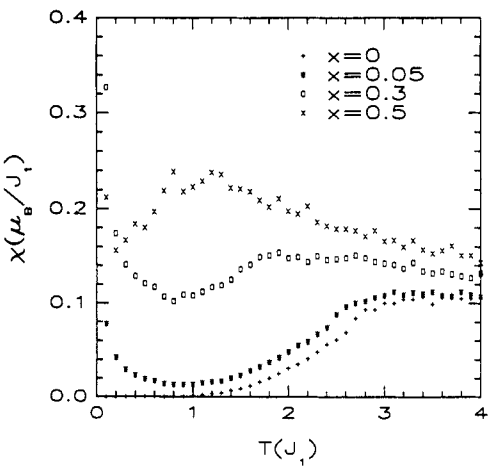

Figure 5. Magnetic susceptibility (per spin) χ versus temperature T for various values of x.

The effects of frustration on the magnetic ordering are clearly seen in the calculated specific heat and order parameters. At $x = 0$, with no frustration, type-I order forms when $T < T_{\mathrm{N}} \approx 2.7J_1$ with $l_{\mathrm{I}} = 1$ and $l_{\mathrm{II}} = 0$. T_{N} is slightly higher than the 2D Ising transition temperature, $T_{\mathrm{N}}^{\mathrm{2D}} \approx 2.27J_1$, representing the effect of the weak interlayer interactions. Two effects occur as x increases. On one hand, dilution of spins and

frustration on the A and C layers result in a lower T_N and a broader transition; on the other hand, more spins develop on the B layers, increasing frustration along the c direction as well as the tendency to form type-II order. At $x \approx 0.3$, the J_3' coupling is still dominant in c direction, so l_I is still larger than l_{II}. By $x = 0.4$, the nature of the 3D AF order begins to change—type-II order appears. Figure 4 shows that, at $x = 0.4$, as temperature decreases, initially l_I grows, then a finite l_{II} appears associated with a small decrease in the value of l_I. This second phase is also seen in the neutron scattering experiments [6]. For larger values of x ($x \approx 0.5$) the joint effect of frustration and dilution is strong enough to eliminate the LRO; the transition becomes very broad with a very low specific heat peak and very small order parameters.

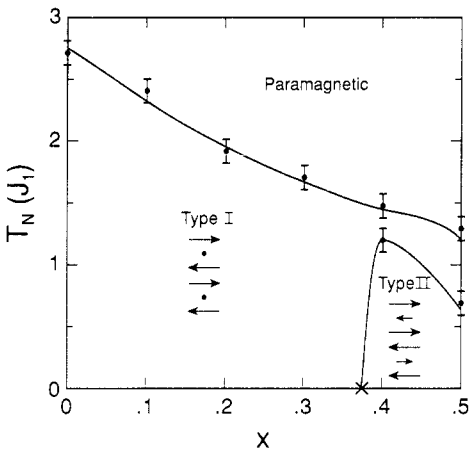

Figure 6. The magnetic phase diagram from MC simulations and the free energy analysis. The shown spin configurations are for two unit cells.

The impact on the magnetic order due to the change in the oxygen content x can be summarized in the phase diagram shown in figure 6, which is in general agreement with the neutron diffraction measurements of Tranquada *et al* [5]. The spin patterns shown are type I and type II respectively, along the c direction. The transition temperature T_N from the paramagnetic to AF state is determined by the peak in specific heat together with the onset of the AF order parameters. The phase boundary, T_N', between I and II is extrapolated from the finite-temperature MC results and the following low temperature calculation.

At T near 0, using the ground state configurations, we can write down the free energy per unit cell, $f = u - Ts$, for type I and II respectively as

$$f_I = -\{[n_{AC}^2\, 4J_1 + n_{AC}^2\, J_2' + (1-n_B)n_{AC}^2\, J_3'] + \tfrac{1}{2}n_B^2\, 4\,[\tfrac{1}{2}x\, J_1 + (1-\tfrac{1}{2}x)J_2]\} - T\,\ln[2^{n_B(1-n_B)^4}]$$

$$f_{II} = -[n_{AC}^2\, 4J_1 + n_{AC}^2\, J_2' - (1-n_B)n_{AC}^2\, J_3'] - n_B\{n_{AC}\, 2J_1' + \tfrac{1}{2}\, n_B\, 4\,[\tfrac{1}{2}x\, J_1 + (1-\tfrac{1}{2}x)J_2]\}$$

where n_{AC} and n_B are the densities of spins in the A (or C) and in the B respectively, and are functions of x. Setting $f_I = f_{II}$ gives the phase boundary

$$T_N'(x) = \frac{2n_{AC}[n_B J_1' - (1-n_B)n_{AC}J_3']}{n_B(1-n_B)^4 \ln 2}. \tag{7}$$

At $T = 0$, the concentration where type I changes to type II, $x_c(T = 0)$, is determined by

$$J_1' n_B = J_3'(1 - n_B) n_{AC}. \tag{8}$$

For J_1', J_3' and the hole distribution given in (5) and (6), we have $x_c(T = 0) = 0.375$. For $T > 0$, the phase boundary slopes to the right, because the totally frustrated spins in the type-I phase generate larger entropy than in type II. This phase boundary therefore corresponds to a *first-order* transition. The co-existence of l_I and l_{II} near the phase boundary is expected in the simulations, as observed. This is also consistent with the co-existence of the two types of spin order observed in neutron scattering [18]

For the calculated magnetic susceptibilities in figure 5, the following unusual features are noticed: (a) the susceptibilities may be decomposed into two parts, a standard AF contribution and a paramagnetic tail at low T, which comes from the frustrated spins on the B layers when the A and C layers are ordered as in type I; (b) as x increases the AF peak in χ becomes very broad with an unobservable cusp at T_N; (c) the paramagnetic tail first grows with increasing x, reaching a maximum at $x \approx 0.3$, then decreases with increasing x. At the maximum ($x \approx 0.3$) the size of the Curie tail corresponds to the number of spins (Cu^{2+}) on the B layers, which is 5.4% of the total number of Cu sites on the B layer, in good agreement with experiment [4, 5]. The reason for the initial increase in the Curie constant comes from the increase in number of frustrated spins on the B layer, which behave like free spins. But as x increases beyond a certain value, type-II AF order involving the B layers develops, most spins on the B layers then become ordered, so the paramagnetic tail is reduced [4].

4. Summary and conclusions

In summary, we would like to discuss how the phase diagram changes if the coupling parameters and spin distribution are different from those in (5) and (6), and thus more generally relate our results to a variety of doped magnetic compounds of the 123 structure. To do so, we have carried out the simulation with different spin distributions with $f = 0$ and $f = 2x$ in (2). We then construct, from these results, a schematic three-dimensional phase diagram with three different cross sections Γ_1, Γ_2 and Γ_3, as shown in figure 7, intersecting the T_N axis ($n_{AC} = 1$, $n_B = 0$) and perpendicular to the n_B–n_{AC} plane. Cross section Γ_1 is the phase diagram of figure 6, with the hole distribution determined by $f = 0.4x$. Cross section Γ_2, within the n_B-T_N plane, is the resulting phase diagram for $f = 2x$ (all the oxygen doping induced holes on the B layers). Cross section Γ_3, within the n_{AC}–T_N plane, is the phase diagram for $f = 0$ (all the oxygen doping induced holes on the A and C layers). The high-T_N at $x = 0.5$ on Γ_2 arises because every Cu site on the B layers has a spin and the system is an ordinary, unfrustrated antiferromagnet. The dotted lines in the n_{AC}–n_B plane are the phase boundaries at $T = 0$: the line parallel to the n_{AC} axis divides type II from type I, while the one parallel to the n_B axis separates the magnetically ordered phase from the paramagnetic phase.

The 3D phase diagram of figure 7 demonstrates the effect of various kinds of doping on the 123 lattice structure. For $YBa_2Cu_3O_{6+x}$, we assumed a simplified oxygen doping hole distribution given by $f = 0.4x$, which gave the phase diagram Γ_1. For a linear relation between f and x with different coefficient, the surface Γ_1 is rotated

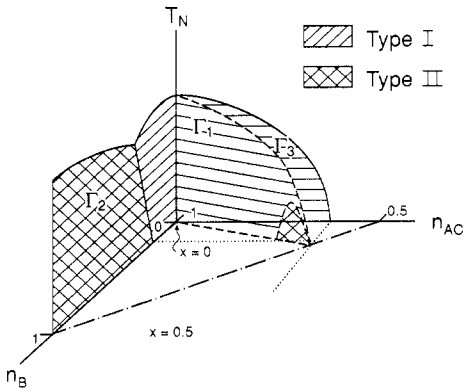

Figure 7. Schematic 3-dimensional phase diagram from MC simulations. n_{AC} and n_B are the number of spins per unit cell on the A (or C) and the B respectively. No oxygen doping, $x = 0$, corresponds to the origin where $n_{AC} = 1$ and $n_B = 0$. The doping concentration $x = 0.5$ is shown as the chain line.

around the T_N axis. The actual relation between f and x is probably not linear [20], with the phase diagram Γ_1 becoming a curved surface. Thus for a given material of 123 structure in which some holes go into A and C while others go into B as x increases, the phase diagram must be a surface lying between the extreme cases Γ_2 and Γ_3, and along which type I changes to type II and then to short-range order.

The cross section Γ_2 is the case where the number of spins on A and C remains as one while the number of spins on B changes from zero to one per unit cell, which approximately describes what happens when Co is substituted for Cu in $YBa_2Cu_3O_{6+x}$: magnetic Co ions replace non-magnetic Cu ions on the B (chain) layers with the A and C layers unchanged resulting in the formation of a type-II phase [21]. The cross section Γ_3 corresponds to the situation where the number of spins on B remains zero while the number of spins on A and C is suppressed; this may apply to doping of Zn into $YBa_2Cu_3O_6$ where non-magnetic Zn^{2+} enters the A and C (plane) layer and replace magnetic Cu^{2+}.

Another interesting case occurs in $NdBa_2Cu_3O_{6+x}$ in which it appears that spins exist in the B layers even at $x = 0$ [7]. Since even stronger anomalies exist in the Ce and Pr analogues [22], a difference in the valence state of Cu due to Nd is not unexpected. The effect amounts in our calculations to a shift of origin to a finite value n_B of spins on the B layers. Thus we would predict that type-II order occurs at low temperatures for $x \approx 0$. At higher temperatures type-I order may or may not occur before the paramagnetic state.

Finally we consider the effects of different values of the J on the the 3D phase diagram. (a) Changing the ratio of the *intralayer* nearest and next-nearest neighbour couplings changes the intralayer frustration, resulting in a different value of x where the LRO disappears; (b) changing the ratio of the *interlayer* nearest and next-nearest neighbour couplings changes the interlayer frustration and results in a different value of x for the boundary between type-I and type-II orders; (c) changing the ratio of an interlayer and the corresponding intralayer couplings changes the degree at which the interlayer frustration affects the T_N, i.e., larger interlayer couplings make the drop of T_N at the boundary of I and II deeper.

The values of J in (5) together with the hole distribution in (6) produce the phase

diagram in figure 6 in which the LRO disappears at $x \approx 0.5$ and type I changes to type II at $x \approx 0.4$. Due to the finite size of a 2D layer in our MC simulation, the interlayer couplings chosen in (5) can not be made as small as suggested by neutron scattering [18,19]†. However, from (c) above, replacing the interlayer couplings by much smaller ones leaves the phase diagram unchanged except for a small overall decrease of T_N, and the elimination of the drop of T_N at the I and II boundary.

In conclusion, Monte Carlo simulations of an Ising model with frustrated spin couplings have accounted for many features of the phase diagram and magnetic ordering in $YBa_2Cu_3O_{6+x}$. Frustration is seen to play an essential role in the magnetic ordering. In addition a more general 3D phase diagram involving independent spin occupations of the chain and plane sites is obtained which relates a number of different doping experiments on the magnetic phase of 123 oxide superconductors.

Acknowledgments

The facilities of the Ohio Supercomputer Center are gratefully acknowledged, as well as support from Air Force/CeramPhysics, Inc. contract AF F4962-86-C-0049. We wish to thank D C Johnston, J W Lynn, J M Tranquada and F Zuo for useful conversations and E Kim for assistance with computing.

References

[1] Liebmann R 1986 *Statistical Mechanics of Periodic Frustrated Ising System* (Berlin: Springer)
Binder K and Young A P 1986 *Rev. Mod. Phys.* **58** 801

[2] Anderson P W 1987 *Science* **235** 1196
Emery V J 1987 *Phys. Rev. Lett.* **58** 2794
Hirsch J E 1987 *Phys. Rev. Lett.* **59** 228

[3] Johnston D C 1989 *Phys. Rev. Lett.* **62** 957
Johnston D C, Goshorn D P, Alvarez M S, Jacobson A J, Lewandowski J T, Newsam J M and Sinha S K *Preprint*

[4] Farneth W E, McLean R S, McCarron,III E M, Zuo F, Lu Y, Patton B R and Epstein A J 1989 *Phys. Rev.* B **39** 6594

[5] Tranquada J M, Moudden A H, Goldman A I, Zolliker P, Cox D E, Shirane G, Sinha S K, Vaknin D, Johnston D C, Alvarez M S, Jacobson A J, Lewandowski J T and Newsam J M 1988 *Phys. Rev.* B **38** 2477

[6] Kadowaki H, Nishi M, Yamada Y, Takeya H, Takei H, Shapiro S M and Shirane G 1988 *Phys. Rev.* B **37** 7932

[7] Lynn J W, Li W-H, Mook H A, Sales B C and Fisk Z 1988 *Phys. Rev. Lett* **60** 2781
Moudden A H, Shirane G, Tranquada J M, Birgeneau R J, Endoh Y, Yamada K, Hidaka Y and Murakami T 1988 *Phys. Rev.* B **38** 8720
Li W-H, Lynn J W and Fisk Z 1990 *Phys. Rev.* B **41** 4098

[8] Birgeneau R J, Skalyo,Jr J and Shirane G 1970 *J. Appl. Phys.* **41** 1303
Birgeneau R J, Als-Nielsen J and Shirane G 1977 *Phys. Rev.* B **16** 280

[9] Shirane G, Endoh Y, Birgeneau R J, Kastner M A, Hidaka Y, Oda M, Suzuki M and Murakami T 1987 *Phys. Rev. Lett.* **59** 1613

† In fact, those listed values of interlayer couplings in (4) are the smallest ones we can put into the simulations. The reason is that when the interlayer coupling(s) multiplied by number of spins in a single layer becomes smaller than temperature, layers will not order with respect to each other. This situation will not occur in a infinite system, where 2D layer size is much larger than 2D correlation length just above T_N.

Endoh Y, Yamada K, Birgeneau R J, Gabbe D R, Jenssen H P, Kastner M A, Peters C J, Picone P J, Thurston T R, Tranquada J M, Shirane G, Hidaka Y, Oda M, Enomoto Y, Suzuki M and Murakami T 1988 *Phys. Rev.* B **37** 7443

[10] Chakravarty S, Halperin B I and Nelson D 1988 *Phys. Rev. Lett.* **60** 1057

[11] Binder K and Stauffer D 1984 *Applications of the Monte Carlo Method in Statistical Physics* ed K Binder (Berlin: Springer)

[12] Lu Y and Patton B R *Preprint*

[13] Jorgensen J D, Beno M A, Hinks D G, Soderholm L, Volin K J, Hitterman R L, Grace J D, Schuller I K, Segre C U, Zhang K and Kleefisch M S 1987 *Phys. Rev.* B **36** 3608

[14] Renault A, McIntyre G J, Collin G, Pouget J P and Comes R 1987 *J. Physique* **48** 1407

[15] Baudelet F, Collin G, Dartyge E, Fontaine A, Kappler J P, Krill G, Itie J P, Jegoudez J, Maurer M, Monod Ph, Revcolevschi A, Tolentino H, Tourillon G and Verdauger M 1987 *Z. Phys.* B **69** 141

[16] Zhang F C and Rice T M 1988 *Phys. Rev.* B **34** 3759

[17] Tranquada J M, Heald S M, Moodenbaugh A R and Suenaga M 1987 *Phys. Rev.* B **35** 7187
Fujimori A, Takayama-Muromachi E, Uchida Y and Okai B 1987 *Phys. Rev.* B **35** 8814

[18] Tranquada J M, Shirane G, Keimer B, Shamoto S and Sato M 1989 *Phys. Rev.* B **40** 4503

[19] Annett J F, Martin R M, McMahan A K and Satpathy S 1989 *Bull. Am. Phys. Soc.* **34** 427, *Phys. Rev.* B **40** 2620

[20] Tranquada J M, Heald S M, Moodenbaugh A R and Xu Y 1988 *Phys. Rev.* B **38** 8893

[21] Miceli P F, Tarascon J M, Greene L H, Barboux P, Giroud M, Neumann D A, Rhyne J J, Schneemeyer L F and Waszczak J V 1988 *Phys. Rev.* B **38** 9209

[22] Yang K N, Dalichaouch Y, Ferreira J M, Lee B W, Neumeier J J, Torikachvili M S, Zhou H, Maple M B and Hake R R 1987 *Solid State Commun.* **63** 515
Chittipeddi S, Song Y, Cox D L, Gaines J R, Golben J P and Epstein A J 1988 *Phys. Rev.* B **37** 7454
Li W-H, Lynn J W, Skanthakumar S, Clinton T W, Kebede A, Jee C-S, Crow J E and Mihalisin T 1989 *Phys. Rev.* B **40** 5300